GFZ
Helmholtz-Zentrum
POTSDAM

Originally published as:

Harris, D., Albaric, J., Goertz-Allmann, B., Kühn, D., Sikora, S., Oye, V. (2017): Interference suppression by adaptive cancellation in a high Arctic seismic experiment. - *Geophysics*, *82*, 4, pp. V201—V209.

DOI: http://doi.org/10.1190/geo2016-0452.1

Interference Suppression by Adaptive Cancellation in a High Arctic Seismic Experiment

D. Harris[1], J. Albaric[2*], B. Goertz-Allmann[2], D. Kuehn[2,3], S. Sikora[4], V. Oye[2]

[1] Deschutes Signal Processing LLC, Maupin, Oregon, USA

[2] NORSAR, Gunnar Randers vei 15, 2007 Kjeller, Norway

[3] GFZ German Research Centre for Geosciences, Helmholtzstr. 6/7, 14467 Potsdam, Germany

[4] CO_2 Lab, The University Centre in Svalbard, P.O. Box 156, 9171 Longyearbyen, Norway

[*] Now at Lab. Chrono-environnement, University of Franche-Comté, 16 route de Gray, 25030 Besançon, France

Email addresses:

D. Harris oregondsp@gmail.com

J. Albaric julie.albaric@gmail.com

B. Goertz-Allmann Bettina.Goertz-Allmann@norsar.no

D. Kuehn daniela@norsar.no

S. Sikora Sebastian.Sikora@unis.no

V. Oye volker@norsar.no

ABSTRACT

Mechanical and electromagnetic interference (process noise) is common in seismic data recorded to monitor and characterize induced microseismicity during industrial injection and production operations. We present a case study of adaptive cancellation to reduce observed process noise in passive seismic data recorded during the 2014 injection test at the CO_2 Lab research site in Spitsbergen. Our results suggest that adaptive cancellation is effective where major sources of interference are readily identifiable. Adaptive cancellation requires these sources to be instrumented separately but conceivably with low-cost sensors. We suggest that adaptive cancellation should be considered routinely when planning microseismic monitoring operations where strong industrial or anthropogenic noise is anticipated. Interference suppression algorithms are sufficiently simple that they could be implemented in acquisition systems to avoid archival of noise reference data.

INTRODUCTION

Monitoring seismicity induced during stimulation and production provides valuable in-situ information about the state of stress in reservoirs, among other parameters. This information is critical not only for the economic success of field development but also for proper assessment of seismic hazard and associated environmental risks. Because dense local instrumentation is employed, the magnitude range of observed reservoir induced events can be very large (below magnitude 0 up to magnitude 5, e.g. in Oklahoma). The signals corresponding to the lower end of the range can have low signal-to-noise ratios (SNR). Noise in oil and gas production fields or

waste product injection sites often is dominated by electromagnetic and mechanical interference, which can obscure seismic signals of interest. Detecting and locating microseismic events in such environments is challenging, particularly for classical techniques that rely upon identification and timing (picking) of relatively clear seismic phases. One can attempt to increase SNR by suppressing process noise with frequency filtering, especially notch filtering for narrowband interference. This approach often comes at a cost of significant waveform distortion and is ineffective against wideband interference. Waveform distortion can, for example, complicate onset picking and parameter estimation (such as moment tensor or magnitude estimation). Another strategy is to employ full-waveform detection and location methods (e.g. backward extrapolation methods, e.g. McMechan, 1982; Lu, 2007; Ringdal and Kværna, 1989; source-scanning algorithms, e.g. Kao and Shan, 2004, Gharti et al., 2010). However, these methods involve stacking or stacking combined with convolution with various kernel functions which are less effective against temporally and spatially correlated noise than against uncorrelated noise. Noise due to industrial processes generally is highly correlated.

From the signal processing perspective, adaptive cancellation is a more satisfactory approach, since it minimizes signal distortion and more effectively reduces interference power. These advantages are compelling for wideband interference and interference with characteristics that change over time, e. g. non-stationary interference. However, adaptive cancellation is not discussed much in the microseismic monitoring literature (Harris et al., 1991; Dragoset, 1995), perhaps because it requires major noise sources to be identified, instrumented and separately recorded. It is not without cost and requires a degree of advance planning. However, with the cost of instrumentation and data archival dropping these disadvantages may become insignificant.

Since adaptive cancellation algorithms are so simple, they can, in principle, be implemented on-site and in real time. This function could be carried out by the archival system itself, eliminating the need for archival of auxiliary noise reference data and subsequent processing. While this approach is a possibility, a conservative operation would archive everything to avoid the any risk of unexpected behavior by the cancellation algorithms.

This paper documents mitigation of noise in seismic recordings due to electromagnetic interference during an injection operation carried out in the summer of 2014 at the CO_2 Lab site in the Adventdalen of Svalbard. The map in Figure 1 shows the location of the injection well Dh5, stations of the seismic network, and the CO_2 Lab building.

The Longyearbyen CO_2 Lab, hosted by the University Centre in Svalbard (UNIS) and a spin-off company, UNIS CO2-lab AS, is a Carbon Capture and Storage (CCS) pilot site. Due to its remoteness and closed energy system comprising a coal-fueled power plant powered by locally mined coal, the Longyearbyen CO_2 Lab project presents a unique opportunity to demonstrate the entire CO_2 value chain from source to geological CO_2 sequestration. The site consists of 8 wells drilled through the permafrost overburden, with the deepest wells reaching about 1000 m depth. The formation considered as potential reservoir consists of sandstone-siltstone layers at 672-970 m depth, overlain by approximately 450 m of cap-rock shale, presenting itself as under-pressured, unconventional reservoir where fluid injectivity is strongly influenced by tectonic fractures (Braathen et al., 2012). One objective of the CO_2 Lab is to promote research based on the combination of geophysical and geological methods for an optimal characterization of the reservoir through time. Several water injection test campaigns have been performed (Braathen et al., 2012).

Recent studies (e.g., Goertz-Allmann et al., 2014) demonstrate that microseismic monitoring is a powerful and cost-effective tool to monitor CO_2 injection and containment. Whereas during the water injection test in 2010 performed at 870-970 m depth in well Dh4, a microseismic event with magnitude M ~ 1 had been recorded and located close to the injection well, later injection tests showed no detectable microseismic events, although pressure and flow rate showed a pattern that is characteristic for fracture opening. We applied adaptive noise cancellation to seismometer data recorded during the 2014 injection, which took place from the 11th to the 13th of August. Our intention was to reduce event detection thresholds or to support the conclusion that the pressure and flow rate pattern may be explained by fracture propagation producing no seismic radiation or slow slip. Water was injected in the Dh5 well, which has an open section between 645 and 701 m. During the 48-hour step rate test, injection rate and pressure varied from 200 to 223 l/min and from 50 to 80 bars, respectively. The site at this time was continuously monitored by eighteen 3-C geophones: 5 situated in shallow boreholes from 7 to 12 m depth (SH, 1.5 Hz sensors), one string of 5 geophones reaching from 100 to 300 m depth (Dh3, 15 Hz sensors) and one string of 8 geophones reaching from 193 to 543 m depth (Dh4, 15 Hz sensors). In addition, one surface 3-C short-period sensor was installed close to the injection pump (LE-3D, 0.2 Hz).

We remark parenthetically that the harsh environment in the high arctic of Svalbard required that the digital recorders be placed in a protected environment. The climate-controlled CO_2 Lab research building was the overwhelmingly desirable choice but had the side-effect of exposing the recorders to strong emitters of electromagnetic interference (EMI). Another undesirable effect on the recordings, which is difficult to avoid in this kind of environment, was improper grounding due to the presence of permafrost.

DATA CHARACTERISTICS

Figure 2 shows spectrograms of earth motion data recorded at a 4 msec sampling interval on the three components of station SH5 roughly mid-day during the injection. All spectrograms in the figure were computed from data recorded in the same two-hour time interval: the top spectrogram is for the vertical component of motion, the middle spectrogram is for the north component and the bottom spectrogram is for the east component. The three spectrograms are rendered to a common intensity scale (expressed as color), allowing direct comparisons of the relative power across all channels. The common scale is normalized to the peak power observed on the three channels, so that 0 dB corresponds to the maximum power present on any of the channels. We will examine the reduction of three types of recorded background noise in this stretch of data: 50 Hz power-line interference, transient electromagnetic interference from the PC used to archive the data, and ground-motion (mechanical) noise propagating to the sensors from the injection pump.

All three types of noise are apparent in Figure 2. The strong vertical line at 50 Hz is contributed by the 220 V power lines present everywhere in the cabin. A second strong EMI emitter (and one less obvious *a priori*) was the laptop PC used to archive and transmit the data. This source produced the regular series of vertical lines spaced at multiples of (approximately) 6.22 Hz, as well as somewhat wider-band transients every minute (horizontal lines). Data were archived by this system in one-minute segments causing the disk to spin up at those intervals and, in turn, producing transient EMI. Finally, the third identified source was the large injection

pump producing a series of lower-frequency lines which stopped about 80% of the way through the record. The lines stop because pumping ceased and the well was shut in.

METHODS

Reduction of recorded interference

We have reported previously on the applied adaptive noise cancellation algorithm (Kühn et al., 2014), but provide more detail here, especially on our approach to reduce multiple independent components of observed interference. Figure 3 shows a trivial (and unworkable) model for noise cancellation. We assume we have a recorded scalar discrete time series $r[i]$ sampling an analog signal $r(t)$, i.e. $r[i] = r(i\Delta t)$ with Δt the sampling interval in seconds and i is the integer time index for the series. We model $r[i]$ as superposition of a desired signal component $s[i]$ and interference $n[i]$. A separate recording $\hat{n}[i]$ of just the noise component is assumed to be available and is subtracted from $r[i]$ to form a residual $\hat{s}[i]$, which is intended to be an estimate of $s[i]$.

This concept is too simple since the noise reference recording $\hat{n}[i]$ almost never is an exact replica of the interfering noise in the primary recording. Often it is distorted by being measured in a different location than the primary sensor (typically close to the noise source). A practical algorithm, widely cited in the signal processing literature [see e.g. Widrow and Stearns (1985), Dragoset (1995), Haykin (2002)] results from modifying the basic notion of subtraction as shown in Figure 4. An adaptive finite impulse response (FIR) filter is employed to shape the noise reference to match the noise component in the primary recording. The filter is chosen to minimize the expected power formed by subtracting the filtered reference from the data. If done accurately, the residual is relatively free of interference. Three conditions must be met for this

scheme to succeed. First, the noise reference must be strongly correlated with the interference in the primary recording. Second, the reference must not have a significant component correlated with the desired signal. Third, enough data must be available to provide numerically well-conditioned estimates of the FIR filter coefficients.

Because the characteristics of noise may drift over time it usually is not possible to estimate the coefficients from a finite sample of data and apply the filter in a static fashion thereafter. For example, careful examination of the lines in Figure 2 originating from the pump shows that the center frequencies vary by tens to hundreds of milliHertz as pumping loads vary (and by significantly more when the pump starts or stops). The same is true, though to a lesser degree, of the power line frequency, which fluctuates as loads are changed on the grid (although carefully regulated by the utility). Because interference is non-stationary the estimates of the coefficients must be updated periodically or even continuously. The Widrow-Hoff algorithm is an effective and simple method to adapt filter coefficients to changing conditions in the data. It does so continuously, i.e. with every time step. The algorithm is summarized by:

$$\begin{aligned} \hat{s}[i] &= r[i] - \sum_{k=-N}^{N} w_k[i]\,\hat{n}[i-k] \\ w_k[i+1] &= w_k[i] + \mu\,\hat{s}[i]\,\hat{n}[i-k]\,; \quad k = -N, \cdots, N \\ w_k[0] &= 0\,;\ \textit{initial condition} \end{aligned} \tag{1}$$

The coefficients are adapted with each time step i by taking a small descent step in the opposite direction of the gradient of the instantaneous power $\hat{s}^2[i]$. The step-size parameter μ controls the size of the descent step, which usually is kept quite small to track slow changes in the data. The elements of the gradient are given by:

$$\frac{\partial \hat{s}^2[i]}{\partial w_k[i]} \;=\; -\left(r[i] \;-\; \sum_{m=-N}^{N} w_m[i]\,\hat{n}[i-m] \right)\hat{n}[i-k] \;=\; -\,\hat{s}[i]\,\hat{n}[i-k]\,; \quad k \;=\; -N, \cdots, N \tag{2}$$

Values of μ usually are chosen empirically. Large values lead to wild and growing oscillations with indeterminate results. Values which are too small result in extremely slow convergence and incomplete interference cancellation. Because the effective step size is influenced by the scale of the noise reference $\hat{n}$, a normalized algorithm often is used (Haykin, 2002), replacing the coefficient update in equation 1 by:

$$w_k[i+1] \;=\; w_k[i] \;+\; \mu\,\frac{\hat{s}[i]\,\hat{n}[i-k]}{\sum_{m=-N}^{N}\hat{n}^2[i-m]}\,; \qquad k \;=\; -N, \cdots, N \tag{3}$$

Values of μ less than about 1 usually give good results in the normalized algorithm.

We choose an initial condition of zero for the filter coefficients $w_k[i]$, which means that initially the algorithm does not modify the primary recording, but gradually phases-in cancellation as the coefficients adapt. This approach causes a start-up behavior where strong interference is not removed until adaptation has proceeded for some time. We also elected to use a two-sided filter (the index on the coefficients ranges from $-N$ to N). This choice automatically corrects minor clock synchronization errors between the reference and primary data recorders. In our experience, the use of an anti-causal filter has not caused unwanted precursors on sharp signal onsets, because the filter is not applied to the primary recording, but rather the noise reference waveform.

As indicated, several independent types of interference exist simultaneously in our data. There are two options for dealing with multiple interference sources. One approach is to extend the cancellation algorithm to update filters simultaneously for multiple interference reference

recordings. The algorithm for doing so is a straightforward extension of equations 1 and 3. Alternatively, one can employ the single-interference cancellation algorithm repeatedly and sequentially to remove one interference source after another. We combined both approaches. Some noise sources, such as 50 Hz lines due to power line EMI are very common in the data, often dominating the reference recordings of other interference sources (e.g. Figure 5). We found it necessary to remove power line interference first, both from the primary seismic data and the remaining interference reference recordings, before cancelling the other sources of interference. On the other hand, we cancelled interference from the pump using the three components of the ground motion reference for that source simultaneously.

Characterizing (recording) interference sources

We employed different instrumentation for each of the three sources of interference. First, we built a simple circuit with a step-down transformer followed by a resistor bridge to reduce power line voltage to the input range of our acquisition system. We recorded this stepped-down voltage as a power line interference reference on one channel of the acquisition system. Figure 5a shows the spectrogram of this reference. Second, we constructed several simple induction coils (Figure 6) of copper wire wound around wooden frames with a capacitive shunt to eliminate very high frequency interference not in our recording band. These EMI pickups were intended to search for, and instrument, other significant sources of EMI in the recording cabin. The data acquisition laptop also shown in Figure 6 was found to produce very significant electromagnetic interference. In the figure, the induction coil is shown resting on the keyboard of the laptop. The spectrogram for the raw recording from the laptop induction coil is shown in Figure 5b, and is seen itself to be dominated by 50 Hz line interference. We applied the

cancellation algorithm to remove the 50 Hz noise from the laptop reference with the result shown in Figure 5c. After cancellation, we see that the laptop generates a large number of narrowband lines spaced at multiples of approximately 6.22 Hz and wider band transients at minute intervals (horizontal lines, noted originally in Figure 2). Third, we deployed a three-component sensor on the surface adjacent to the main injection pump to collect reference waveforms for ground motion caused by the pump during the injection.

The pump reference deployment is depicted in Figure 7. Figure 8 shows spectrograms for the pump reference channels (Z, N, E) during the same two-hour period and frequency range (0-60 Hz) as shown for the primary seismometer channel in Figure 2. Note the highly non-stationary line components of ground vibration as the pump's revolutions per minute (rpm) varied with changing load conditions or while it was adjusted by the operator. In addition, the three components of ground motion responded differently to the numerous excitations of the pump (and possibly other pieces of equipment on the site), raising the possibility that a multiple-reference form of the cancellation algorithm may (automatically) separate and target these various components of interference. The very large number of interference components suggests that it would have been desirable to have even more independent recordings of the injection equipment. Interference from the pump is a concern primarily for primary instrumentation at relatively small offsets from the injection site. We noted that instruments deployed a kilometer or more away showed relatively little interference, due to attenuation of these wavefield components, which propagate principally as surface waves. The instruments at small offsets, however, are crucial to detection of low-level seismicity.

Deployment of the pump reference highlights an important question regarding the cancellation idea: if the cancellation reference contains a component of the desired waveform (e.g. a microseism) won't cancellation reduce the target waveform as well as the intended interference? It can, but the damage to the target waveform will be negligible if the power of the reference is dominated by the intended interference. In practice, this requirement should be easy to meet by placing the reference sensor(s) very close to the source of interference. Since it is the very weak signals that we seek to detect through the aid of cancellation, the surface expression of those signals should be orders of magnitude below the interference ground motion.

RESULTS

Progressive cancellation of interference in the primary seismic data

After some experimentation we determined the most effective approach to interference reduction in these data sets to be progressive cancellation of noise sources in order of their dominance in the power spectrum. In the following presentation of cancellation, we focus on a single data channel (from station SH5, east component) which was representative of results for those primary seismic recordings with noise dominated by the three types of interference for which we had reference recordings. We used the normalized update algorithm of equation 3 with $N = 150$ and $\mu = 0.1$. Figure 9 shows the results of progressively cancelling interference. The first step was to remove the 50 Hz interference from the power line using the reference of figure 5a. The result (Figure 9b) is near complete removal of the 50 Hz line interference and some suppression of the (approximate) 6.22 Hz multiple from the laptop (which must be correlated with the line frequency). In subsequent processing, we determined that such a

large value of N is unnecessary in the case of cancellation of a single pure tone (the 50 Hz interference in these data). We changed N to 1, so that only 3 coefficients are used in a canceler for power line interference. This seems to work well and there is less chance for mischief with all the extra degrees of freedom.

Figure 9c shows the results of cancelling the noise from the laptop using the reference signal from Figure 5c operating on the cancellation residual from the first step (9b). These results are more impressive, showing nearly complete suppression of the 6.22 Hz multiples across the spectrum. Finally Figure 9d shows the result of pump noise cancellation on the residual trace corresponding to 9c. In this case, the cancellation algorithm was modified to use simultaneously the three reference recordings of Figure 8 (corresponding to the traces recorded on the three components of the sensor). Simultaneous cancellation was appropriate in this case for two reasons: the power of the three reference recordings was roughly balanced and simultaneous use of the references allowed the cancellation algorithm to exploit correlations among the narrowband components of pump noise apparent in Figure 8 for improved noise rejection.

Figure 9d shows imperfect cancellation, which is a result of the simplified time-adaptive algorithm used to estimate the cancellation filter coefficients $w_k[i]$. It took some time for the coefficients to adapt to the interference especially for the very strong line around 4 Hz and the sharp transient near the bottom of the spectrogram near 20 Hz. Consequently, some of the power from the pump interference appears in the residual. This behavior was not apparent in the two earlier steps, in part because there were three times as many coefficients to constrain in this step (because there were three reference traces), which may have slowed the adaptation process. We observe that the start-up transient behavior of the algorithm (resulting in initial leakage of the

low-frequency line) could have been avoided with continuous operation of the canceller over days of data.

In addition, the cancellation is not perfect because we had only one sensor to deploy on the surface near the pump. Although we refer to the interference source as a "pump", in fact there were several, possibly many, motors and rotating machines on site. In principal, one can cancel only as many independent sources of noise as there are reference recordings. Deployment of more reference sensors probably would have resulted in a more thorough removal of interference in the data.

Tests of signal preservation

One of the claims made for cancellation is that it preserves the character of desired transients better than conventional (e.g. frequency-filtering) processing methods. It also is the case that competing conventional methods for rejecting complicated interference can become quite complex, and involve significant analyst intervention (thus raising the cost of post-processing analysis). We illustrate these points with a synthetic example obtained by superimposing a signal recorded on the vertical component of station SH1 from a microseism that occurred during the 2010 injection experiment at the CO_2 Lab [Kühn et al., 2014] upon background noise recording during the 2014 campaign.

Figure 10 contrasts the results of two processing strategies: conventional frequency-filtering to remove the interference and cancellation. The noise in this case also was recorded on SH1 Z, but in 2014 consisted wholly of ambient electromagnetic interference, since no instrument was present on the input channel. To reduce the noise with conventional filtering, we constructed a 50 Hz notch filter with a bandwidth of 1 Hz, and a cascade of filters with notches

at multiples of (approximately) 6.22 Hz. These eliminate noise components due to the power line and the EMI produced by the laptop (refer to the EMI components of background evident in Figure 2). The left side of Figure 10 shows the original microseismic signal embedded in noise (top) and the results of applying the 50 Hz notch filter (middle) and additionally the cascade of 6.22 Hz notch filters (bottom). Clearly very significant noise rejection is achieved in these two filtering steps: -23.4 dB for the 50 Hz notch and an additional -2.8 dB for the subsequent cascade of notch filters. However, the penalties paid are substantial "ringing" in the resulting microseismic waveform that might interfere significantly with onset picking, and the complexity of designing and applying the cascade of notch filters.

By contrast, the right side of Figure 10 shows again the original signal (top) and the cancellation residuals obtained with the power line reference (middle) and additionally the laptop reference (bottom). In this example, a much simpler canceler was used for rejection of the 50 Hz line; the number of canceler coefficients was drastically reduced ($N = 1$) and the adaptation rate parameter (μ) was reduced to 0.01. The large number of coefficients ($N = 150$) in the earlier examples was found to be overkill for noise dominated by one narrow line and actually degraded performance slightly. The original parameters were retained for the laptop canceler. For the cancellation results, the noise rejection is substantial again: -23.3 dB and -3.4 dB respectively for the 50 Hz and laptop reference cancelers. The laptop canceler performs better than the cascade of notch filters since there is more to the laptop EMI than just the periodically-spaced lines. The cancellation algorithms notably produce a clean onset to pick on the microseism, since the residuals lack the ringing caused by the notched filters, which are very sharp in the frequency domain to avoid too much loss of signal energy. We observe that once the laptop reference is obtained (by instrumenting the laptop with the coil of Figure 6), subsequent processing to reduce

the noise observed from the laptop is much simpler than design and application of the cascade of notch filters. This is a general observation; interference can be quite complex and wideband making it difficult or impossible to eliminate with simple filtering approaches. But cancellation approaches largely avoid the complexity once the interference source is found and properly instrumented.

The cancelers also produce a better result in the frequency domain. Figure 11 contrasts the results in the energy spectra of the signals. The figure top panel overlays the spectrum of the original microseism recording (black) with the spectrum of the notch filter output (red; obtained from the transform of the bottom trace in the left panel of Figure 10). The periodic holes in the spectrum of the notch filter output are avoidable spectral bias. The bottom panel overlays the spectra of the original signal (black) again with the signal estimated by the cancelers (red). Note that the additional nulls in the spectrum are absent. Both processed spectra show greater variability than the original signal spectrum and higher levels in the low- and high-frequency tails. These effects are due to residual noise (added to the microseism) not removed by the either of the processing techniques. The cancellation algorithm adds somewhat more noise to the high-frequency portion of the spectrum, which we suspect is due to numerical noise in the coefficient update process (equation 3). The level of this noise is insignificant (60 dB below the peak signal spectrum).

Test of detection threshold

Another question that arises naturally is how much the detection threshold might be improved with cancellation. This question is difficult to answer in general because it depends on the nature of the noise and how easy it is to identify and instrument the

sources. Each recording venue will be unique. To explore this question for our particular venue, we again buried the 2010 microseism recording in background noise at different levels of scaling. This process is illustrated in Figure 12. The top trace shows the background noise recorded by the vertical channel of station SH4, with copies of the (M_L ~1, local magnitude, see e.g. Deichmann, 2006 for a definition of this scale) microseism superimposed at -5 dB increments of amplitude scaling (corresponding to decrements of 0.25 in M_L) starting at -15 dB (M_L ~0.25). Because the 2010 microseism and the 2014 noise observation were recorded with the same instruments and recorders, it is a valid construction of event observations at specified magnitude levels. Station SH4 was close to the injection point and the noise it observed was dominated by the pump. Laptop EMI was present, but 50 Hz interference was not significant (so 50 Hz cancellation was not used in this example).

The second trace in the figure shows the residual following cancellation using the 3 pump references of Figure 8. The canceler reduced the background noise level by 11.2 dB. In addition, the laptop EMI reference was used to cancel the residual and resulted in another 1 dB of noise rejection. The final residual (bottom trace of Figure 12; pump + EMI cancellation) shows more clearly defined transients, including a hint of the microseism at a -40 dB scale factor. One could say from this example that cancellation improved the detection threshold by close to 10 dB (0.5 change in M_L) without recourse to conventional frequency filtering. This process would result in preservation of the maximum bandwidth in observed microseisms.

Of course, the use of judicious frequency filtering can improve signal-to-noise (SNR) ratios and reduce detection thresholds. Figure 13 (top trace) shows detail of the original

signal filtered with a 15 Hz highpass filter, which significantly (5 dB) improves the SNR of the microseism observations. Combining frequency filtering with cancellation (bottom 2 traces of Figure 13) results in even more gains, to the point where the microseism scaled at -45 dB is just barely visible (though not reliably detectable). The net result of Figures 12 and 13 is that a detection threshold of M_L -1 might have been possible at this site with cancellation, which is an increment in M_L of perhaps 0.5 lower than what would have been possible without cancellation.

CONCLUSION

The most significant result of this experiment in interference cancellation is that we achieved a substantial reduction of noise from ground vibration due to the pump. The EMI rejection obviously was significant as well, but EMI can be ameliorated also with increased shielding and grounding (though grounding is difficult in permafrost). It is more difficult to provide mechanical isolation for the pumps than it is to instrument them with accelerometers. Furthermore, it is costly after the fact to remove industrial process or other anthropogenic noise without noise reference recordings. Analysts must take time to examine the structure of noise and devise a "conventional" processing approach to attempt to remove it. Such an approach is less likely to be successful for complex wideband noise which may be non-stationary. By contrast, cancellation using recorded noise references is easy to apply and may reduce the power of even highly-complicated, non-stationary, wideband noise, provided the references are well chosen.

The observation that our surface reference recording of pump ground motion could have been more comprehensive highlights an experimental design tradeoff: what fraction of recording bandwidth should be devoted to the primary mission of seismic recording versus the auxiliary

interference recording function? As the cost of recording additional channels drops, it may be that a significant number of channels could be devoted to characterizing interference sources, particularly if cancellation is anticipated significantly to enhance the SNR of primary data channels. It is not necessary to use high-quality instrumentation (as we did for the pump in the Adventdalen) for interference measurements, as noise levels obviously are very high in proximity to the pump. Inexpensive, low-gain sensors are perfectly adequate, provided the reference waveforms remain in the linear region of the transducer. In future, where the cancellation option could be part of experimental design and all data telemetered or cabled to a central recording location, cancellation could be carried out as part of the archival function. The cancellation algorithms are simple and computationally inexpensive, well within the capacity of modern field microprocessors. If cancellation were integrated into the archival function no recording bandwidth would be lost to auxiliary interference characterization. However, until the cancellation option is thoroughly evaluated it might be preferable to record the primary and auxiliary (noise reference) channels separately, as we did here.

The Widrow-Hoff algorithm has the disadvantage of slow adaptation, which was responsible for the sluggish response to the strong pump line around 4 Hz between 12:00 and 12:20 in Figure 9d and possibly remaining start-up transients from the laptop sometimes just visible. These defects might be ameliorated with use of a more sophisticated algorithm ,e.g. recursive least squares, (Haykin, 2002), though at the cost of greater computational complexity and possibly some distortion of desired transient signals. That possibility is a subject for further research.

We remark in closing that we systematically applied the techniques described in this paper in an automated fashion to the entire dataset recorded during the 2014 injection at the CO_2 Lab

site. No microseismicity was observed so the cancellation operations in this case served only to reduce an upper bound on the threshold (magnitude) of observation, perhaps by 0.5 magnitude unit. At the same time, the fact that no microseismic events were detected during injection of these relatively small water volumes decreases the likelihood that CO_2 storage at the CO_2 Lab site will be endangered by induced or triggered seismicity, especially since the amount of CO_2 produced by the local power plant is significantly lower than the quantities to be stored at other industrial sites.

ACKNOWLEDGEMENTS

The work was financed by Norwegian Research Council grant no. 224880 (SafeCO2-II project). The project was sponsored additionally by our industry partners Lundin, RWE DEA Norge and Statoil. The authors thank Michael Roth for providing the LE3D seismometer used to instrument the injection pump and for help with setup, data retrieval, and general training on the Geode data recorders, Dominik Lang for providing one of the Geode recorders and the archival PC, Rune Paulsen for testing the GPS, Jan Fyen, Paul Larsen and Vidar Dohli for consultation on design of sensors for recording the power line and EMI and for giving us access to a lab and parts for building the power line sensor.

REFERENCES

Braathen, A., Balum, K., Christiansen, H.H., Dahl, T., Eiken, O., Elvebakk, H., Hansen, F., Hanssen, T.H., Jochmann, M., Johansen, T.A., Johnsen, H., Larsen, L., Lie, T., Mertes, J., Mork, A., Mork, M.B., Nemec, W., Olaussen, S., Oye, V., Rod, K., Titlestad, G.O., Tveranger, J. and Vagle, K.,2012, The Longyearbyen CO2 Lab of Svalbard, Norway—initial assessment of the geological conditions for CO2 sequestration: Norwegian Journal of Geology, **92**, 353-376.

Deichmann, N. 2006, Local magnitude, a moment revisited, Bulletin of the Seismological Society of America, **96**(4A) pp. 1267-1277.

Dragoset, B. 1995, Geophysical applications of adaptive-noise cancellation, SEG Technical Program Expanded Abstracts, pp. 1389-1392.

Gharti, H. N., Oye, V., Roth, M. & Kühn, D., 2010, Automated microearthquake location using envelope stacking and robust global optimization: Geophysics **75**, MA27–MA46.

Goertz-Allmann, B. P., Kühn, D., Oye, V., Bohloli, B., & Aker, E., 2014, Combining microseismic observations and geomechanical models to interpret storage integrity at the In Salah CCS site: Geophysical Journal International, **198**, 447-461.

Harris, D. B., S. P. Jarpe, P. E. Harben, 1991, Seismic noise cancellation in a geothermal field: Geophysics, **56**, 1677-1680.

Haykin, S., 2002, Adaptive Filter Theory: Prentice Hall.

Kao, H., and S. J. Shan, 2004, The source-scanning algorithm: Mapping the distribution of seismic sources in time and space: Geophysical Journal International, **157**, 589–594.

Kühn, D. V. Oye, J. Albaric, D. Harris, G. Hillers, A. Braathen, S. Olaussen, 2014, Preparing for CO2 storage in the Arctic – Assessing background seismic activity and noise characteristics at the CO2 Lab site, Svalbard: Energy Procedia, **63**, 4313-4322.
DOI: 10.1016/j.egypro.2014.11.467

Lu, R., 2007, Time-reversed acoustics and applications to earthquake location and salt dome flank imaging: Ph.D. thesis, Massachusetts Institute of Technology.

McMechan, G. A., 1982, Determination of source parameters by wavefield extrapolation: Geophysical Journal of the Royal Astronomical Society, **71**, 613–628.

Ringdal, F., and T. Kværna, 1989, A multi-channel processing approach to real time network detection, phase association, and threshold monitoring: Bulletin of the Seismological Society of America, **79**, 1927–1940.

Widrow B., and S. D. Stearns, 1985, Adaptive Signal Processing: Prentice Hall, Englewood Cliffs, NJ, ISBN-0130040290.

LIST OF FIGURES

bottom right deployed on the keyboard of the data acquisition laptop. The data acquisition recorders are located in the cases to the right.

Figure 7 Deployment of a dedicated sensor to collect a three-component reference signal for pump interference. On the left, the view shows the cabin, the pump and associated tank for injection fluids behind the sensor, which is indicated by a white arrow (LE-3D on Figure 1). On the right, a different view shows the sensor in the clear plastic box. The large metal chest contains the recorder.

Figure 8 Spectrograms of 2 hours of pump noise collected on the surface next to the pump by the dedicated 3-component sensor. Note that the three sensor components are differently sensitive to the various components of the noise. The line spectra vary in frequency as the pump responds to different conditions of load and is adjusted by the operator to run at different rates (rpm). The spectrograms are rendered to a common scale with 0 dB referred to the peak power of all channels.

Figure 9 Spectrograms showing progressive removal of interference from the data stream of station SH5, east component: (a) original data, same as Figure 2 bottom image, (b) after suppression of 50 Hz interference, (c) following suppression of the laptop EMI and (d) after cancellation of pump ground motion. The spectrograms are rendered to a common scale with 0 dB referred to the peak power of all channels.

Figure 10 Cancellation produces less waveform distortion to a microseism than processing with notch filters. The left panel shows the waveform of the 2010 microseism scaled (by 0.02) and superimposed on electronic noise recorded on channel SH1 Z (top) and the results of filtering with a 50 Hz notch filter (middle) and a cascade of 6.2+ Hz notch filters (bottom). The right

panel shows the original superposition again (top) and the results of the 50 Hz canceler (middle) and laptop EMI canceler (bottom). The notch filters predictably produce a ringing precursor which could interfere with picking.

Figure 11 Notch filters produce more distortion of the signal spectrum than cancellation. The top panel compares spectra the original 2010 microseism clip with the result after superposition on electronic noise and notch filtering to remove (most of) the noise. The repetitive notches (0.5 Hz wide) at approximately 6.22 Hz intervals and a broader (~1.0 Hz) notch at 50 Hz distort the signal spectrum. The bottom panel compares the original spectrum with the spectrum that results after cancellation. The spectrum after cancellation tracks the original better in the high-energy portion of the spectrum. The low energy tails of the two processed spectra exhibit more variability and higher levels due to the effect of additive noise not completely removed by the processing.

Figure 12 Cancellation improves detectability of a microseism buried in recorded noise. The top trace shows the waveform of the 2010 (~M_L 1) microseism buried, at various scales, in ground motion and electronic noise recorded on the vertical channel station SH4. The microseism was recorded on SH1 (vertical channel) with very high SNR, then scaled in increments of -5 dB, starting with -15 dB. In this case, the background noise is dominated by ground motion noise from the pump, but also has electromagnetic interference. Following cancellation of the pump noise (middle trace), the microseism is visible at two additional scales. Cancellation of the laptop EMI in addition to the pump interference (bottom trace) provides slightly lower background and better definition of transient signals, including one due to a passing vehicle visible between 160 and 180 seconds.

Figure 13 Cancellation improves microseism detectability over frequency-filtering alone. The top trace shows the 2010 microseism embedded in the same noise recording as in figure 12, but filtered with a 5-pole 15 Hz highpass filter. The highpass operation reduces the detection threshold by about -5 dB. The two stages of cancellation reduce the threshold by at least another -5 dB. If these results are representative, the post-processing detection threshold might be as low as M_L -1.

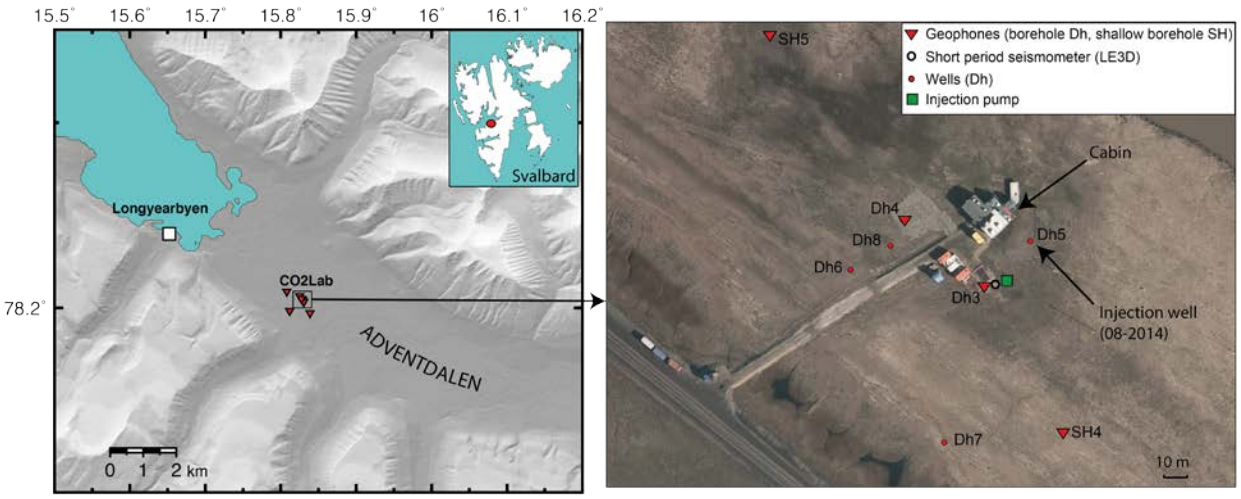

Figure 1 Map of the CO_2 Lab site in Adventdalen**,** Svalbard, Norway (aerial photograph from the Norwegian Polar Institute).

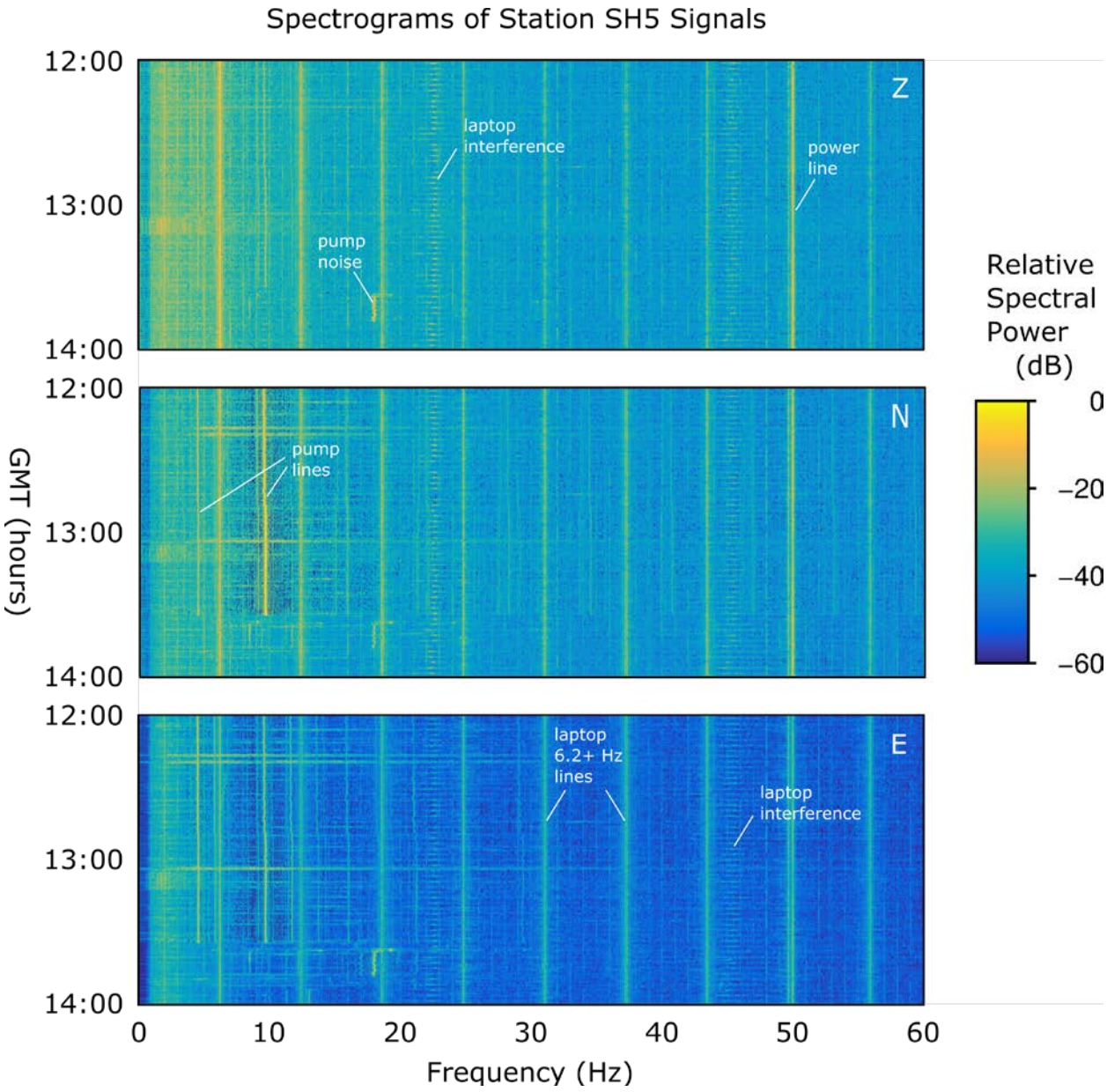

Figure 2 Spectrograms of two hour recordings of ground motion at the three components of station SH5 (vertical, Z, component of motion at top, north, N, component in the middle, east, E, component at bottom). Several types of interference are present, ranging from 50 Hz power line noise to periodic noise from the recording personal computer and lower-frequency pump noise (lines which stop about 80% of the way through the record). The spectrograms are rendered to a common scale with 0 dB referred to the peak power of all channels.

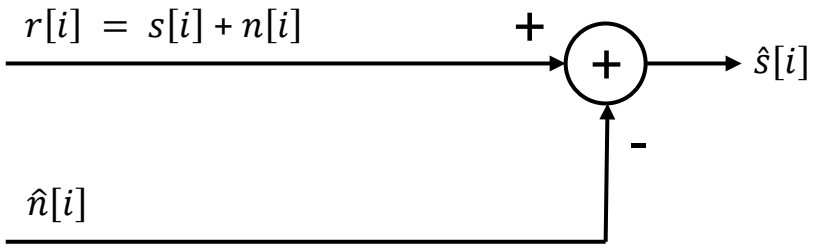

Figure 3 The basic idea behind cancellation: subtraction of an independent ("noise reference") recording $\widehat{\boldsymbol{n}}[\boldsymbol{i}]$ of the interference $\boldsymbol{n}[\boldsymbol{i}]$ superimposed on the desired signal $\boldsymbol{s}[\boldsymbol{i}]$ to cancel the interference in the "primary" recording $\boldsymbol{r}[\boldsymbol{i}]$. The problem with this scheme is that usually $\widehat{\boldsymbol{n}}[\boldsymbol{i}] \neq \boldsymbol{n}[\boldsymbol{i}]$.

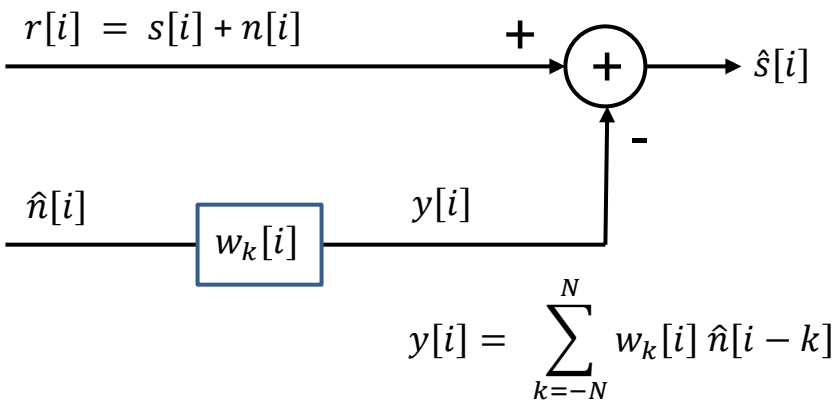

Figure 4 The Widrow-Hoff algorithm filters the interference reference $\hat{\boldsymbol{n}}[\boldsymbol{i}]$ to match the interference present in the recorded data stream $\boldsymbol{r}[\boldsymbol{i}]$.

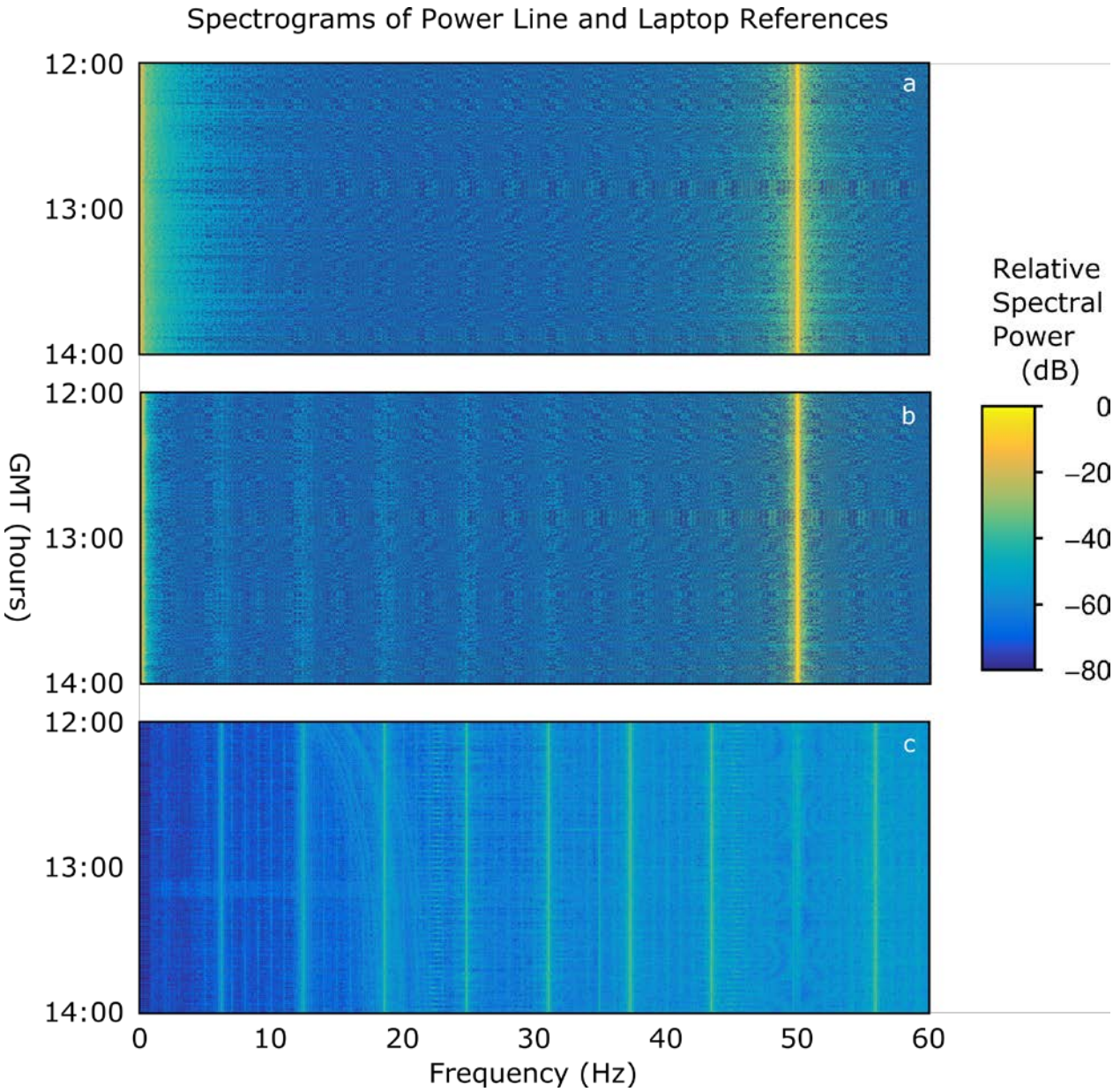

Figure 5 Spectrograms of the reference recordings for electromagnetic interference: (a) 50 Hz power line reference, (b) laptop EMI reference of Figure 6, (c) result of removing the 50 Hz component from (b). The horizontal "ripples" in the spectrograms (a) and (b) are artifacts resulting from sidelobes of the temporal window used in the spectrogram routine. The spectrograms are rendered to a common scale with 0 dB referred to the peak power of all channels.

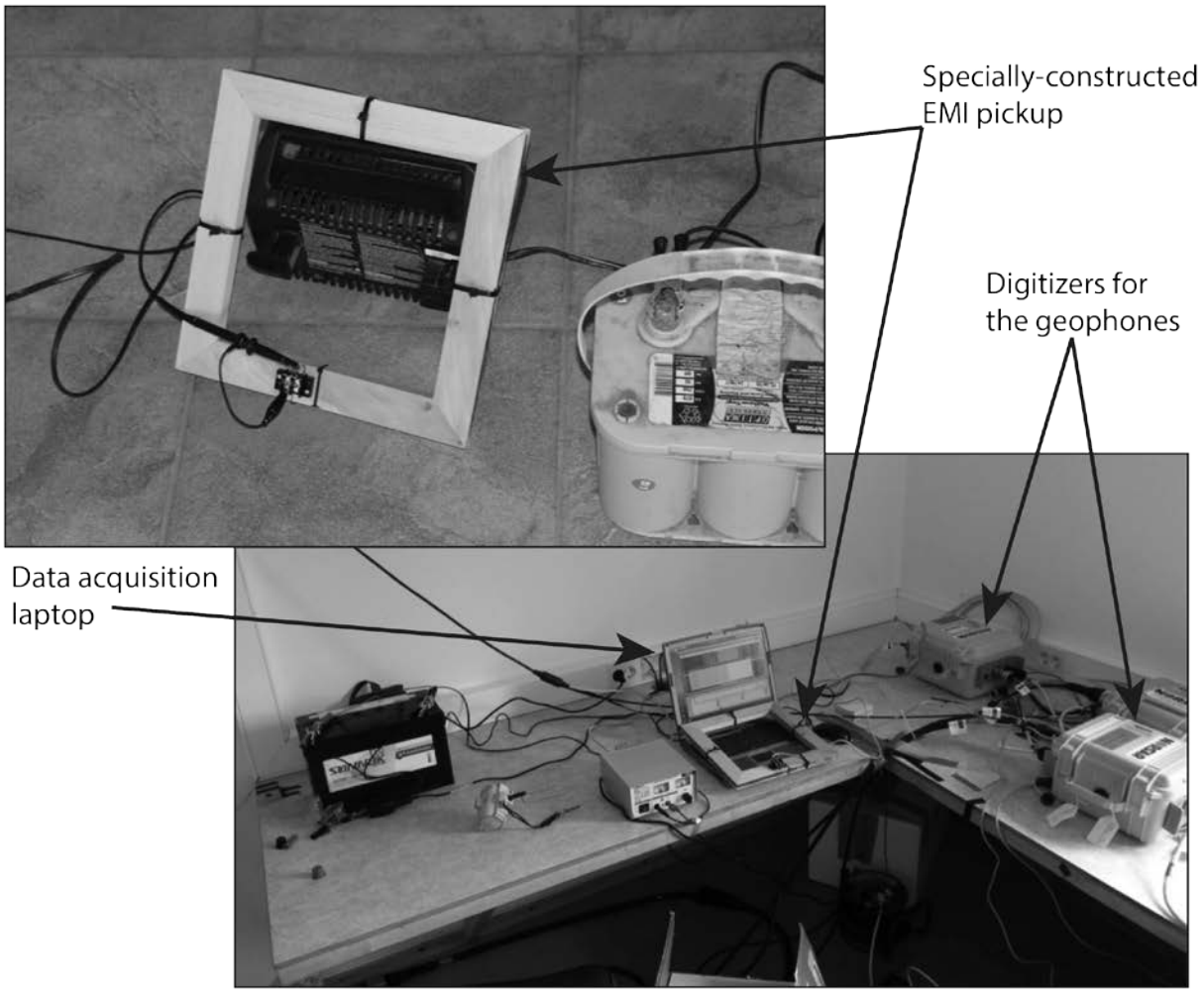

Figure 6 Induction coils designed to search for and instrument EMI in the CO_2 Lab cabin. The image at top left shows a coil being tested on a noisy battery charger. Another coil is shown at bottom right deployed on the keyboard of the data acquisition laptop. The data acquisition recorders are located in the cases to the right.

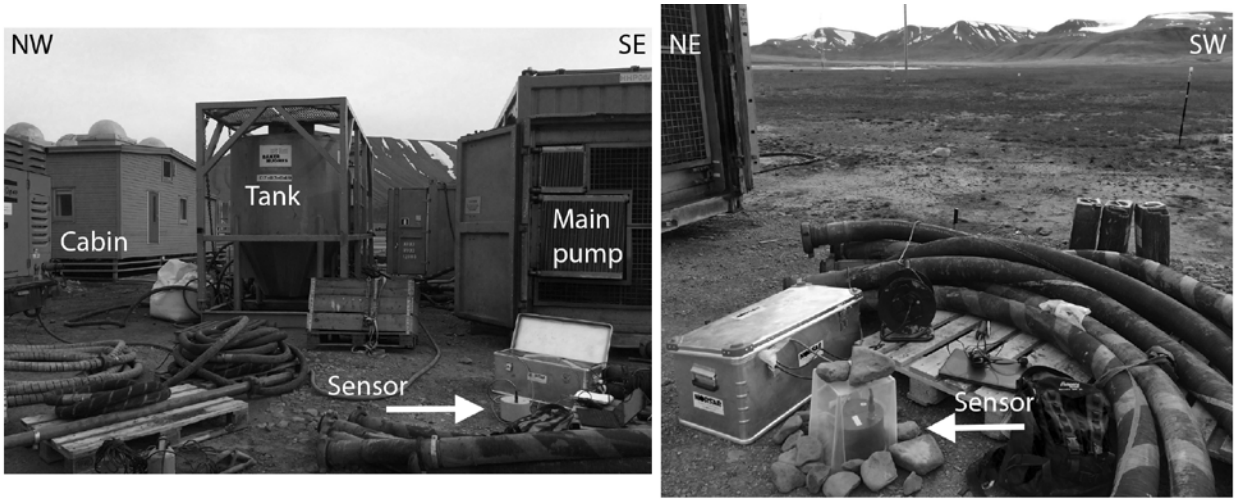

Figure 7 Deployment of a dedicated sensor to collect a three-component reference signal for pump interference. On the left, the view shows the cabin, the pump and associated tank for injection fluids behind the sensor, which is indicated by a white arrow (LE-3D on Figure 1). On the right, a different view shows the sensor in the clear plastic box. The large metal chest contains the recorder.

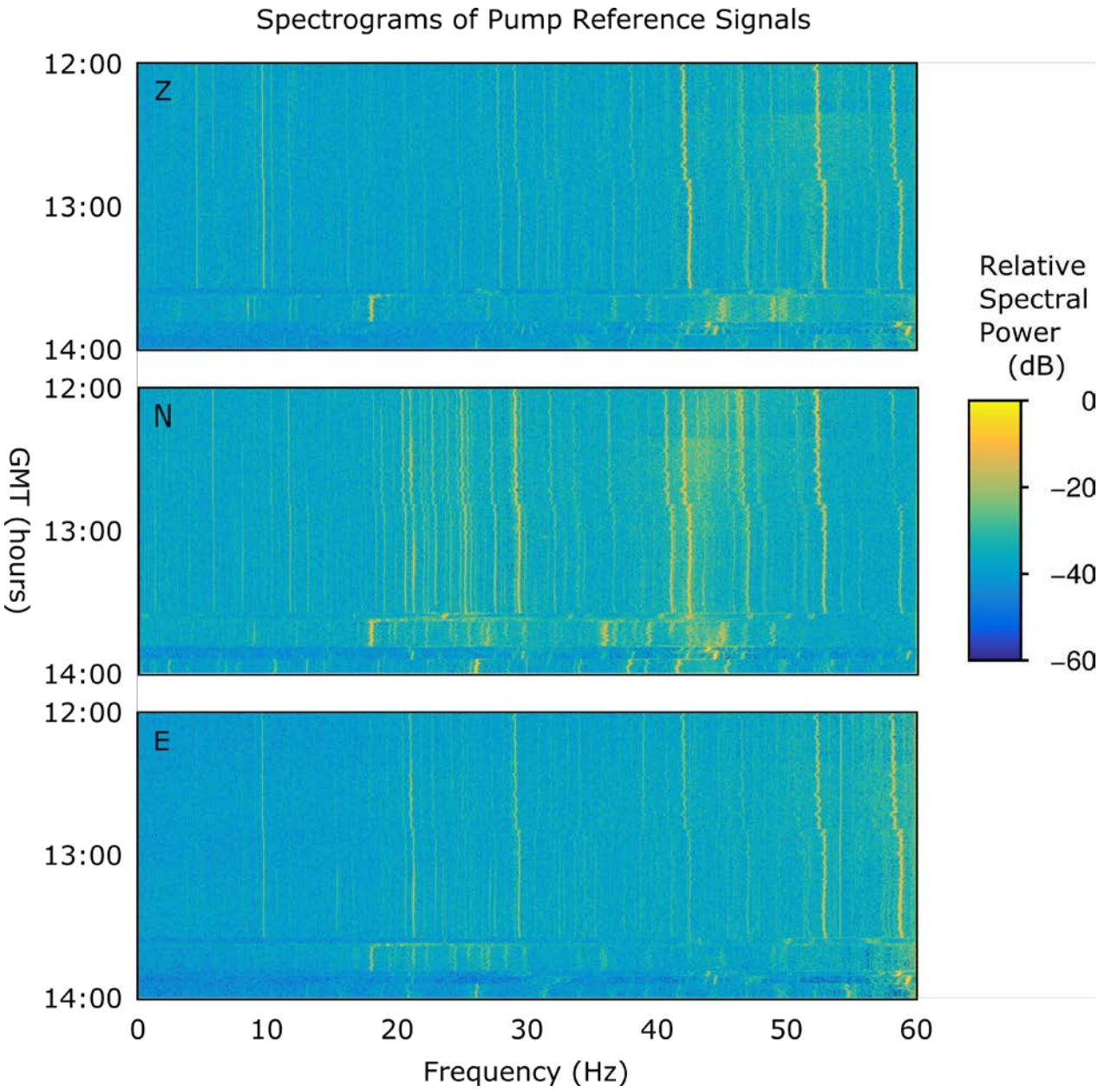

Figure 8 Spectrograms of 2 hours of pump noise collected on the surface next to the pump by the dedicated 3-component sensor. Note that the three sensor components are differently sensitive to the various components of the noise. The line spectra vary in frequency as the pump responds to different conditions of load and is adjusted by the operator to run at different rates (rpm). The spectrograms are rendered to a common scale with 0 dB referred to the peak power of all channels.

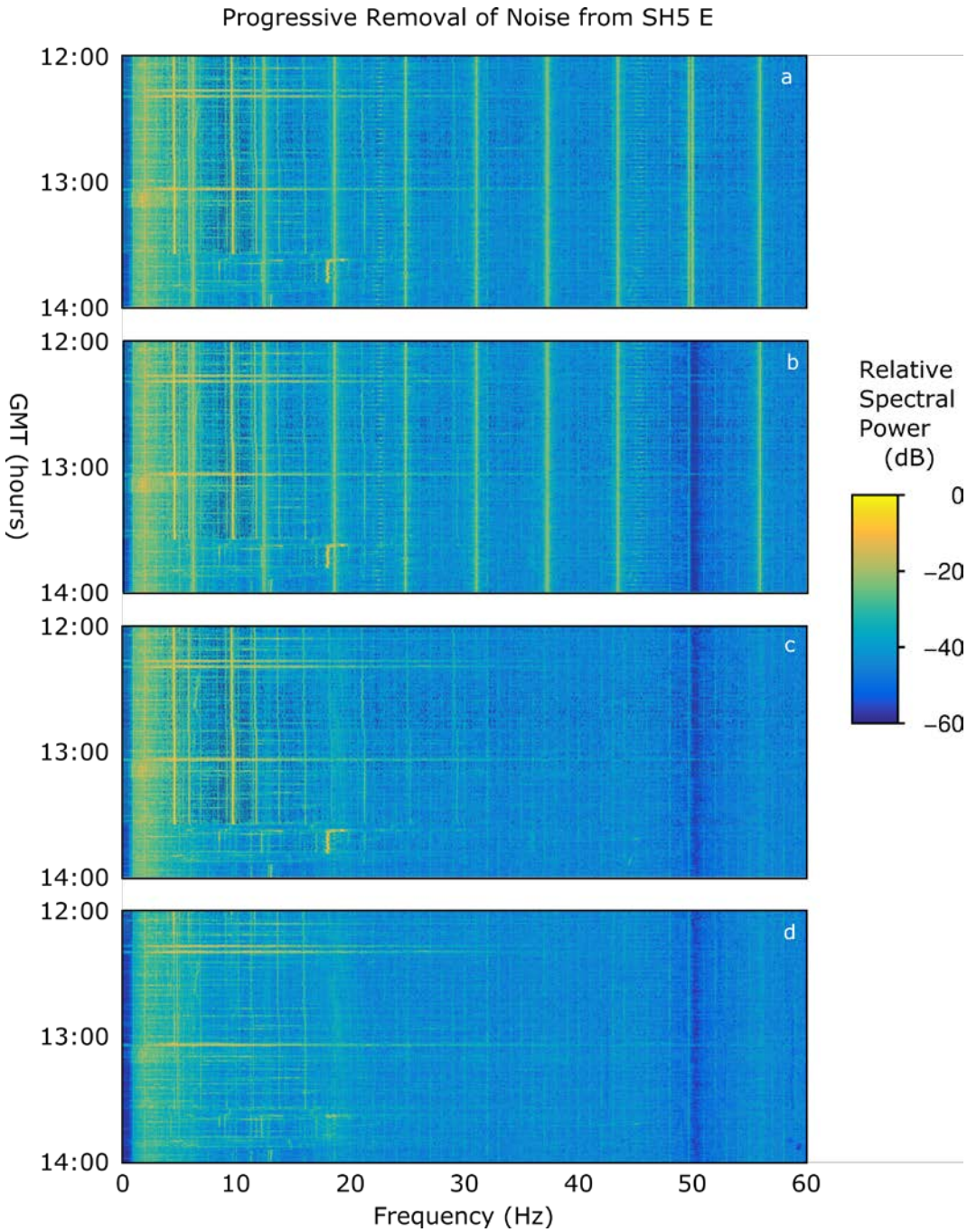

Figure 9 Spectrograms showing progressive removal of interference from the data stream of station SH5, east component: (a) original data, same as Figure 2 bottom image, (b) after suppression of 50 Hz interference, (c) following suppression of the laptop EMI and (d) after cancellation of pump ground motion. The spectrograms are rendered to a common scale with 0 dB referred to the peak power of all channels.

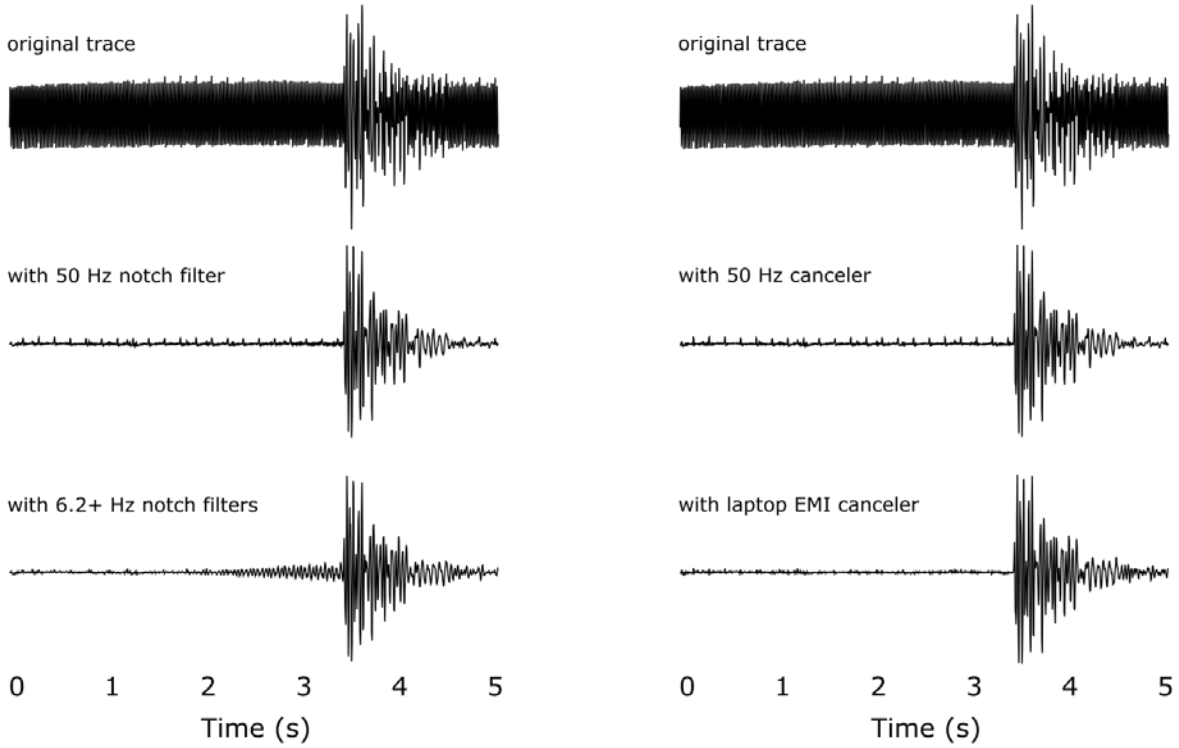

Figure 10 Cancellation produces less waveform distortion to a microseism than processing with notch filters. The left panel shows the waveform of the 2010 microseism scaled (by 0.02) and superimposed on electronic noise recorded on channel SH1 Z (top) and the results of filtering with a 50 Hz notch filter (middle) and a cascade of 6.2+ Hz notch filters (bottom). The right panel shows the original superposition again (top) and the results of the 50 Hz canceler (middle) and laptop EMI canceler (bottom). The notch filters predictably produce a ringing precursor which could interfere with picking.

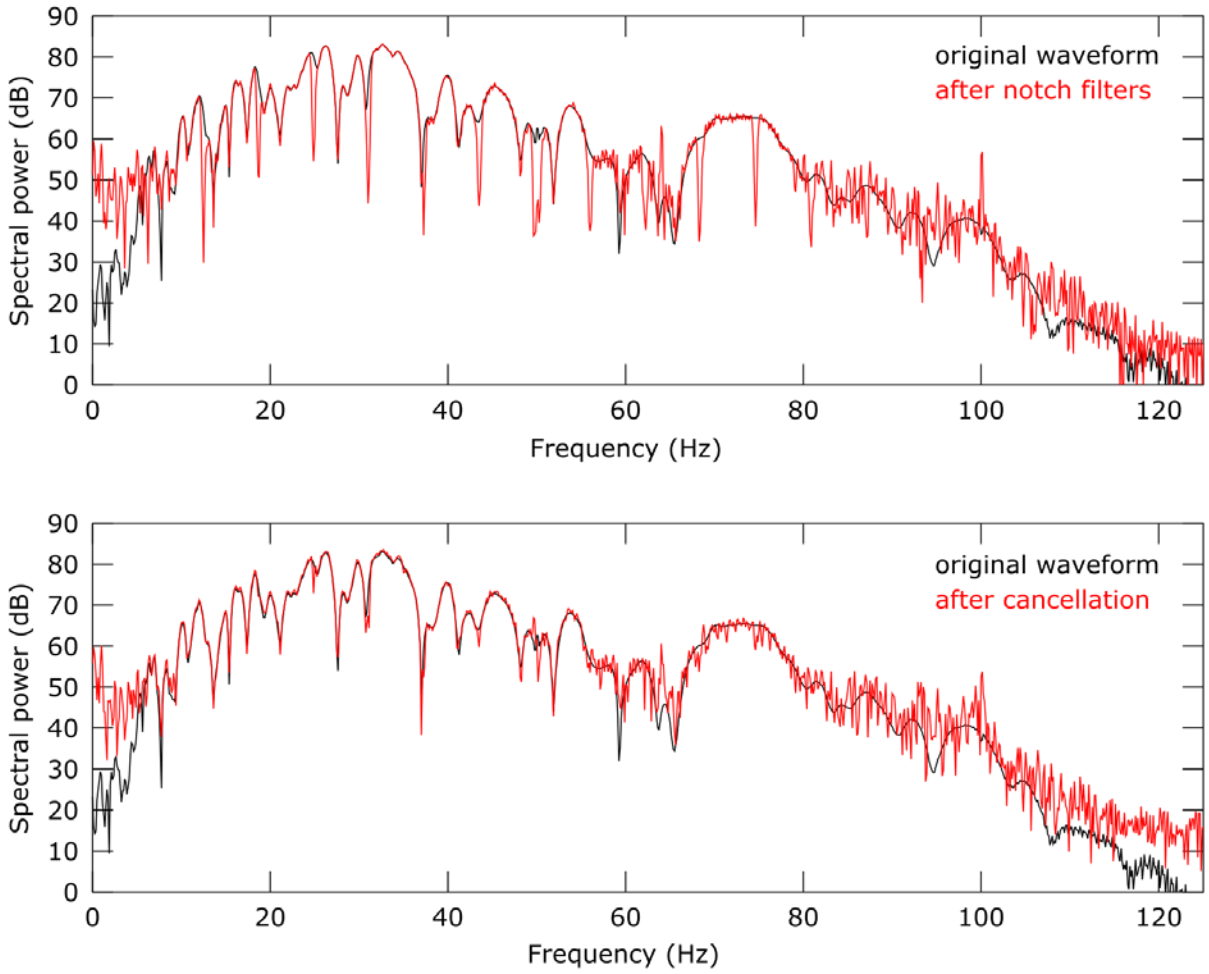

Figure 11 Notch filters produce more distortion of the signal spectrum than cancellation. The top panel compares spectra the original 2010 microseism clip with the result after superposition on electronic noise and notch filtering to remove (most of) the noise. The repetitive notches (0.5 Hz wide) at approximately 6.22 Hz intervals and a broader (~1.0 Hz) notch at 50 Hz distort the signal spectrum. The bottom panel compares the original spectrum with the spectrum that results after cancellation. The spectrum after cancellation tracks the original better in the high-energy portion of the spectrum. The low energy tails of the two processed spectra exhibit more variability and higher levels due to the effect of additive noise not removed by the processing.

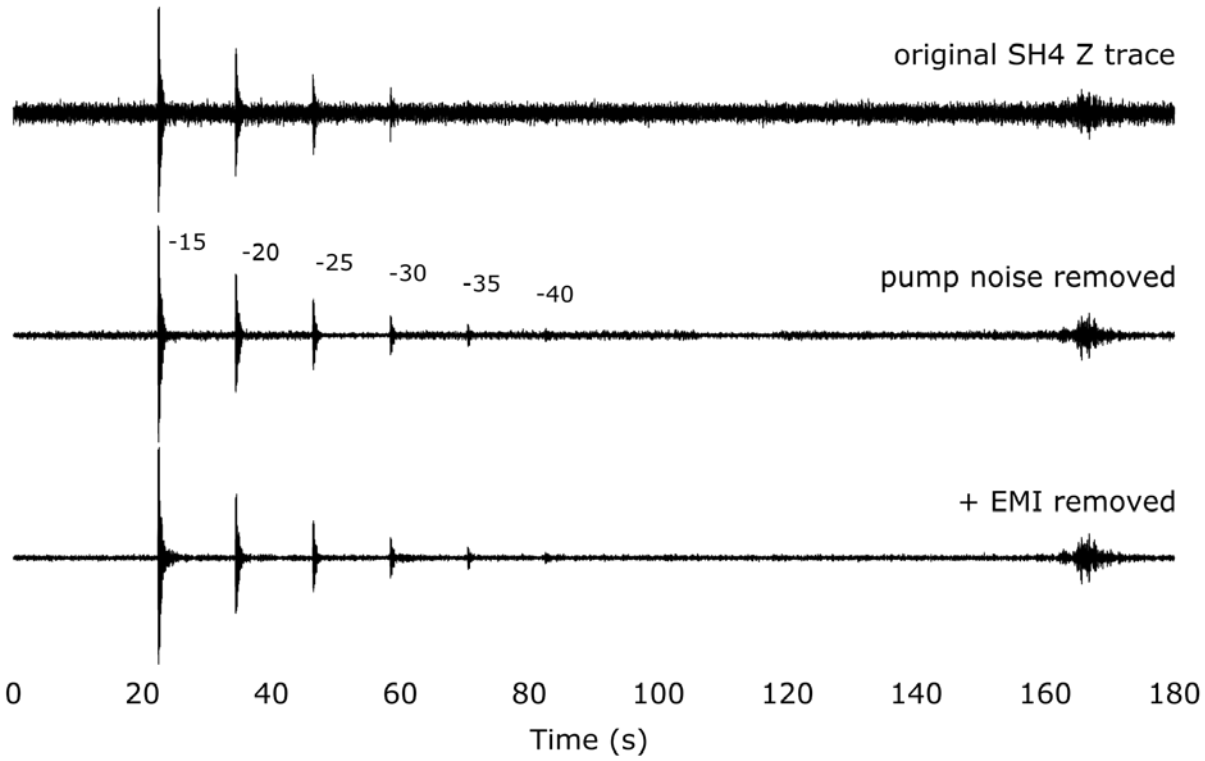

Figure 12 Cancellation improves detectability of a microseism buried in recorded noise. The top trace shows the waveform of the 2010 (~M_L 1) microseism buried, at various scales, in ground motion and electronic noise recorded on the vertical channel station SH4. The microseism was recorded on SH1 (vertical channel) with very high SNR, then scaled in increments of -5 dB, starting with -15 dB. In this case, the background noise is dominated by ground motion noise from the pump, but also has electromagnetic interference. Following cancellation of the pump noise (middle trace), the microseism is visible at two additional scales. Cancellation of the laptop EMI in addition to the pump interference (bottom trace) provides slightly lower background and better definition of transient signals, including one due to a passing vehicle visible between 160 and 180 seconds.

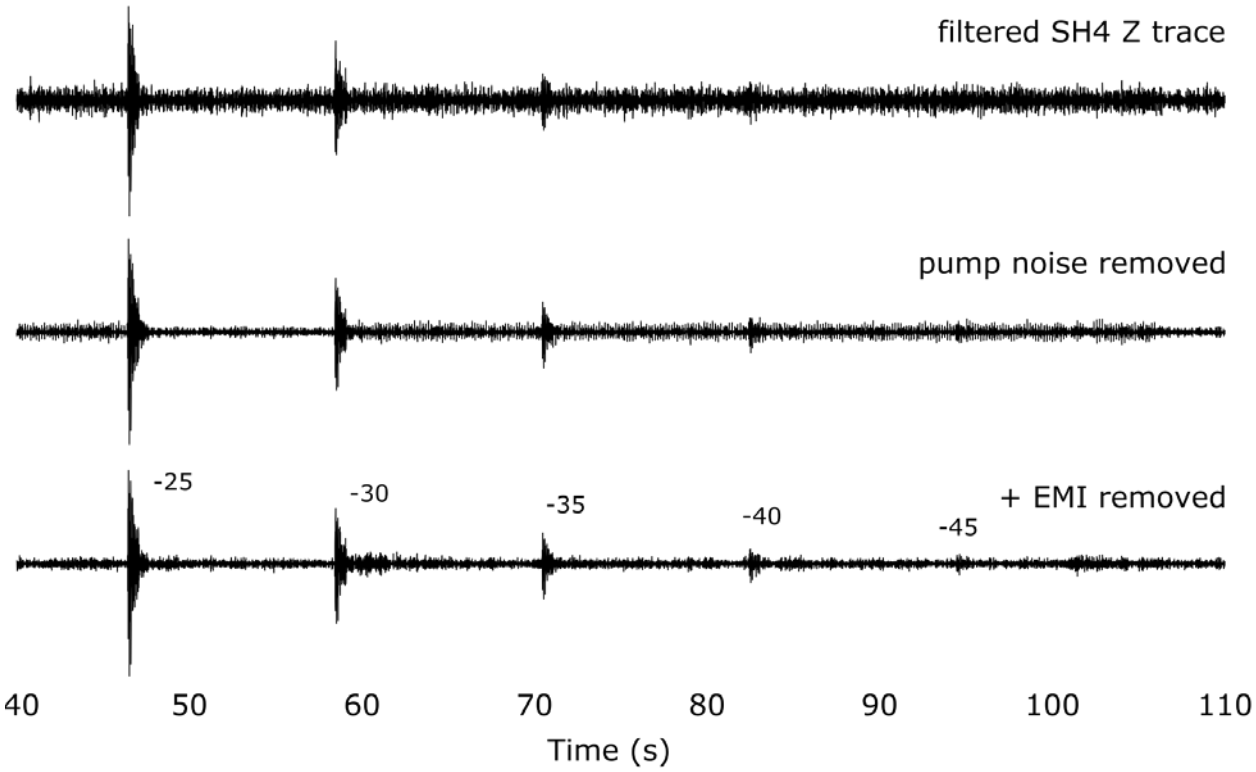

Figure 13 Cancellation improves microseism detectability over frequency-filtering alone. The top trace shows the 2010 microseism embedded in the same noise recording as in figure 12, but filtered with a 5-pole 15 Hz highpass filter. The highpass operation reduces the detection threshold by about -5 dB. The two stages of cancellation reduce the threshold by at least another -5 dB. If these results are representative, the post-processing detection threshold might be as low as M_L -1.